Spin dynamics of $S = 2$ triangular and honeycomb lattices

Anna Reuß,[1] Vadim Ksenofontov,[1] Julia Menten,[1] Reinhard K. Kremer,[2] and Angela Möller[1,*]
[1]*Department of Chemistry, Johannes Gutenberg-Universität Mainz, Duesbergweg 10-14, Germany*
[2]*Max Planck Institute for Solid State Research, Stuttgart, Heisenbergstrasse 1, Germany*

(Received 30 March 2020; revised manuscript received 24 April 2020; accepted 28 April 2020; published 14 May 2020)

Spin dynamics of $S = 2$ triangular and honeycomb lattices realized in $BaNa_2Fe[VO_4]_2$ and $BaNa_2Fe_{2/3}Mg_{1/3}[VO_4]_2$, respectively, are investigated by magnetization, heat capacity, and particularly ^{57}Fe Mössbauer spectroscopy measurements from which spin fluctuation rates are derived. Slight distortions of the $[FeO_6]$ polyhedra from D_{3d} symmetry probe the respective anisotropy of the electronic ground state. $BaNa_2Fe[VO_4]_2$ and $BaNa_2Fe_{2/3}Mg_{1/3}[VO_4]_2$ reveal magnetic decoupling of the underlying magnetic lattices. Down to the lowest temperature of our experiments (3.3 K) only the triangular lattice exhibits long-range order ($T_c = 6.5$ K). The long-range order involves only 2/3 of the Fe sites (static, $H_{hf} \approx 190$ kOe), and 1/3 of the Fe sites fluctuate faster than the observation time window of the Mössbauer spectroscopy experiment. For the honeycomb lattice two distinct iron sites alternate. The moments oriented within the plane slow down considerably with $H_{hf} \approx 120$ kOe whereas the moments on Fe sites aligned along the c axis retain a three times larger fluctuation frequency. In both cases the orthogonal moments, obtained from the orientation of the hyperfine fields with respect to the electric field gradient, couple through Dzyaloshinskii-Moriya interaction. Magnetization data for both compounds show signs of ferromagnetic alignment of the reduced moments, M(0 kOe) $\approx 2\ \mu_B$ per Fe. The evaluation of the specific heat data and Mössbauer spectra for the $BaNa_2Fe[VO_4]_2$ supports the presence of short-range antiferromagnetic interactions below 50 K and suggests a crossover into competing ferromagnetic exchange below 10 K preceding the emerging long-range order.

DOI: 10.1103/PhysRevB.101.184414

I. INTRODUCTION

Low-dimensional frustrated magnetic systems on the triangular (TL), honeycomb (HL), and kagome (KL) lattices [1] have been in the focus of the search for unconventional magnetic ground states. Theoretical work and current experiments on model systems probing relevant factors that enhance strong quantum fluctuations with relevance to quantum spin liquids (QSL) are summarized in Refs. [2–4]. Aspects of spin-orbit coupling are discussed in Ref. [5]. At present, the rational synthesis of QSL candidates and the unambiguous experimental evidence to distinguish these from spin-glass or spin-gel materials [6,7] remain a challenging task.

The concept of frustration is inherent to the antiferromagnetic TL [8] and has been widely studied since. Two cases can be distinguished. Most common are materials of the distorted TL type with collinear long-range order (LRO). Contrary, the undistorted TL (crystal structures with robust threefold symmetry) exhibit the noncollinear 120° Néel state and magnetic LRO at finite temperatures [9], e.g., the $S = 5/2$ XY-Heisenberg TL compounds $RbFe[MoO_4]_2$ [10] and $AAg_2Fe[VO_4]_2$ with A = K, Rb [11]. Recently, the impact of the A-site cation on the magnetic order has been investigated for the $S = 3/2$ series $AAg_2Cr[VO_4]_2$ with A = Ag, K, Rb. For the smallest A-site cation, A = Ag, collinear LRO ($T_N = 10$ K) on the moderately distorted TL is established whereas the undistorted TL members evade LRO down to 25 mK [12]. This surprising finding suggests that unconventional excitations evidenced by μ-SR spectroscopy experiments are involved in the latter QSL candidates [13]. Along this line, the possibility of spontaneous decays in the spin dynamics were considered in a more general context by theory and inelastic neutron experiments [14,15].

Intriguing are the degrees of freedom that control the magnetic ground state of a TL: (i) spin-orbit coupling possibly inducing uniaxial magnetism, (ii) small local distortions that arise from size effects, e.g., A-cation or tetrahedral linker (VO_4^{3-} vs PO_4^{3-}), and (iii) static vs dynamic effects (Jahn-Teller theorem [16]) arising from the anisotropies of the spin system in the presence of unquenched orbital momenta. As an example, the Co compounds of the glaserite-type materials [17] exhibit ferromagnetic LRO ($BaAg_2Co[VO_4]_2$) [18] whereas for $BaNa_2Co[PO_4]_2$ no magnetic ordering down to 0.05 K was reported [19]. This suggests that local distortions of the $[MO_6]$-polyhedra (M = magnetic ion) tune the ratio of ferromagnetic and antiferromagnetic exchange in these insulating materials. Enhanced spin fluctuations are expected when both exchange couplings are balanced. Furthermore, under the condition of weak spin coupling, the possibility of magnetic decoupling for integer spins on the TL is considered [20–23]. As an example, Ag_2MnO_2 shows a frustration-inducted spin-glass-like behavior which originates from symmetry breaking of the triangular lattice to $S = 2$ chains [24–26].

*Corresponding author: angela.moeller@uni-mainz.de

In order to suppress strong magnetoelastic effects detected by neutron diffraction experiments, e.g., in Ag_2MnO_2 [24] or VOCl [27] we consider glaserite-type compounds to provide a more rigid support of the TL and HL through bridging diamagnetic tetrahedral entities. ^{57}Fe Mössbauer spectroscopy allows the microscopic probing of spin fluctuations in the magnetic state on time scales ($\approx 10^{-8}$ s) [28], faster than neutron diffraction experiments used to determine the magnetic structures. The questions we address here relate to the induced dynamics by (i) anisotropy (weak spin-orbit coupling), (ii) noncollinear antiferromagnetic vs ferromagnetic exchange, and (iii) spin decoupling on TL and HL derivatives. We selected the slightly distorted TL compound $BaNa_2Fe[VO_4]_2$ ($S = 2$) for which initial work revealed insight into the structural phase transition in the paramagnetic region and the magnetic structure investigated by neutron diffraction data [29,30].

To distinguish the magnetic exchange for different slight local distortions of the $[FeO_6]$-polyhedra present, we compare the TL with the bipartite HL ($BaNa_2Fe_{2/3}Mg_{1/3}[VO_4]_2$) and comment briefly on the inverted HL ($BaNa_2Fe_{1/3}Mg_{2/3}[VO_4]_2$) in the Appendix. Examples for HL's of the glaserite-type compounds, with $S = 1$ (Ni^{2+}) and $S^{eff} = 1/2$ (Co^{2+}) have been previously reported [31]. Recently, noncollinear antiferromagnetic order on the HL with integer spins has been analyzed in terms of Dzyaloshinski-Moriya interaction (DMI) [32,33] arising from spin-orbit coupling for $Ni_2Mo_3O_8$ containing Ni^{2+} ($S = 1$) magnetic ions [34].

The work is organized as follows: First we discuss structural details of the respective local distortions of the $[FeO_6]$ polyhedra present in $BaNa_2Fe[VO_4]_2$ (TL) and $BaNa_2Fe_{2/3}Mg_{1/3}[VO_4]_2$ (HL). Then we proceed to Mössbauer spectroscopic results resolving electronic and magnetic dynamics along with the discussion of magnetization and specific heat data.

II. EXPERIMENTAL

A. Synthesis

Powder samples of $BaNa_2Fe[VO_4]_2$ (TL) were prepared by solid-state techniques using stoichiometric amounts of $BaCO_3$ (99.8%; Alfa Aesar), Na_2CO_3 (99.5%, anhydrous; Acros), $FeC_2O_4 \cdot 2\,H_2O$ (99%; Alfa Aesar), and V_2O_5 (99.2%; Alfa Aesar) according to the procedure described in Ref. [29]. $BaNa_2Fe_{2/3}Mg_{1/3}[VO_4]_2$ (HL) was obtained by an analogous synthesis route using $BaCO_3$, Na_2CO_3, V_2O_5, $FeC_2O_4 \cdot 2\,H_2O$ and $Mg(OH)_2$ (99%; Fluka). $Mg(OH)_2$ and $FeC_2O_4 \cdot 2\,H_2O$ were used in a ratio of 1:2 in this case.

B. X-ray diffraction

The purity of the samples was verified by quantitative phase analysis via Rietveld refinements [35] of x-ray powder diffraction data collected on a STADI-P (STOE & Cie) diffractometer in transmission geometry (monochromatic Mo-$K\alpha_1$ radiation, $\lambda = 0.7093$ Å). Low-temperature experiments were conducted using a Cryostream 800 (Oxford). $BaNa_2Fe[VO_4]_2$ (TL) crystallizes in the space group $P\bar{3}$ ($Z = 1$; $a = 5.5626(1)$ Å and $c = 7.1003(2)$ Å at room temperature and below 273 K in the monoclinic space group $C2/c$ ($Z = 4$) with refined lattice parameters at $T = 98$ K: $a = 9.5434(2)$ Å, $b = 5.6013(2)$ Å, $c = 14.1257(3)$ Å and $\beta = 90.379(2)^\circ$. $BaNa_2Fe_{2/3}Mg_{1/3}[VO_4]_2$ (HL) can be refined in the trigonal space group $P\bar{3}$ ($T = 298$ K: $a = 5.5554(1)$ Å, $c = 7.0925(2)$ Å; $T = 123$ K: $a = 5.5361(1)$ Å, $c = 7.0786(2)$ Å) and in the entire temperature range from 310 K to 115 K with similar R values in the space group $C2/c$ [$T = 298$ K: $a = 9.6280(6)$ Å, $b = 5.5520(4)$ Å, $c = 14.1843(8)$ Å, $\beta = 90.000(7)^\circ$; $T = 123$ K: $a = 9.609(1)$ Å, $b = 5.536(7)$ Å, $c = 14.171(1)$ Å, $\beta = 90.00(2)^\circ$]. Within the experimental resolution of our xrd data no structural phase transition is observed.

C. ^{57}Fe-Mössbauer spectroscopy

Mössbauer spectroscopic data were collected at temperatures between room temperature and 3.3 K using a custom build setup including a closed cycle cryostat (C2, Montana Instruments). α-iron foil was employed as a standard. Measurements in zero field and in an applied magnetic field of about 1 T created by NdFeB permanent magnets were carried out. To avoid texture effects, the samples were prepared with paraffin as a homogenizing neutral medium. Small impurities of Fe_3O_4 (<5% Fe-site population) are resolved at the lowest temperatures. The Mössbauer spectra were analyzed using the software Recoil [36]:

(i) Paramagnetic spectra were fitted by Lorentzian line shape analysis, providing the following parameters: the chemical shift (CS), quadrupole splitting ($QS = \frac{e^2qQ}{2}/\sqrt{1+\eta^2/3}$), the line width ($w$), and fractions of subspectra (distinguishable iron sites).

(ii) Magnetic spectra were fitted using the full static Hamiltonian approach which additionally provides the sign of the quadrupole splitting QS, the asymmetry parameter η, the hyperfine magnetic field at the nucleus H_{hf}, and θ_{hq}. The latter describes the angle between hyperfine field and the main axis V_{zz} of the electric field gradient (EFG).

(iii) In the magnetic fluctuating region the spectra were fitted using a dynamical line shape model with: H_{hf}, θ_{hq}, the quadrupole shift ϵ, and the fluctuation frequency f of the magnetic hyperfine field flipping parallel to the main axis of the EFG [37,38]. Especially in the fast fluctuating regime, strong correlations between the hyperfine field and the relaxation frequency exist and are inherent to the dynamic model [37,38]. Here we used the fixed values of the magnetic hyperfine field H_{hf}, derived from the full static Hamiltonian site analysis to estimate the respective fluctuation frequencies f. At temperatures where the fluctuations slow down and the system transits into the static magnetically ordered state, H_{hf} and f can be fitted simultaneously.

(iv) We prepared oriented powder samples by embedding the HL compound in a slow hardening epoxy resin in an applied magnetic field of 1 T perpendicular to the absorber plane at room temperature, for reference see Ref. [39]. Mössbauer spectra with the γ radiation aligned parallel to the unique axis of the oriented paramagnetic sample were recorded at temperatures between 100 K and 200 K. The sign of the quadrupole splitting ($e^2qQ/2$) can then be deduced from the

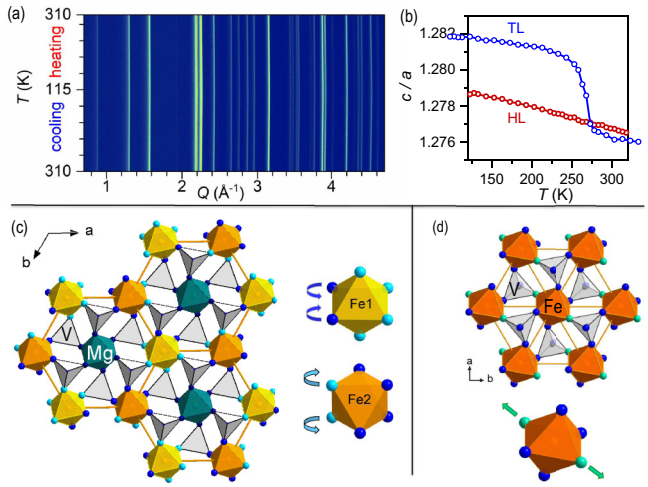

FIG. 1. (a) Contour plot of the projected intensity of x-ray diffraction patterns as a function of temperature for $BaNa_2Fe_{2/3}Mg_{1/3}[VO_4]_2$ (HL). (b) Temperature dependence of the c/a lattice parameter ratio for $BaNa_2Fe[VO_4]_2$ (TL) and $BaNa_2Fe_{2/3}Mg_{1/3}[VO_4]_2$ (HL). (c) HL layer and angular distortion of the two $[FeO_6]$ entities. (d) TL layer and the axial distortion of the $[FeO_6]$ entity.

spectral area asymmetry of the two lines belonging to each quadrupole doublet [40].

Due to the stacking of TL and HL layers along the c axis and all Fe sites exhibiting only minor—but distinct—deviations from D_{3d} symmetry, we assume an axial field (V_{zz}) parallel to the EFG with $\eta \approx 0$. Provided that the hyperfine magnetic interaction dominates the quadrupole one, $\epsilon = e^2qQ/8[2 - (3 - \eta\cos^2\phi_{hq})\sin^2\theta_{hq}]$ can be approximated by $\epsilon = e^2qQ/4$ ($\theta_{hq} = 0°$) and $\epsilon \approx -e^2qQ/8$ ($\theta_{hq} = 90°$).

D. Magnetization measurements

The field dependence of the magnetization was measured in applied fields up to 7 T using a MPMS-SQUID magnetometer (Quantum Design) and a physical property measurement system (Cryogenic), respectively.

E. Specific heat measurements

The heat capacity of TL was measured in zero magnetic field between 1.8 and 130 K with a physical property measurement system (Quantum Design).

III. RESULTS AND DISCUSSION

A. Crystal structures

$BaNa_2Fe[VO_4]_2$ (TL) and $BaNa_2Fe_{2/3}Mg_{1/3}[VO_4]_2$ (HL) both belong to the glaserite type of compounds [17,41] with magnetic ions (Fe^{2+}) in distinct different local symmetries (Fig. 1). In both cases the magnetic layers (TL and HL) are separated by Ba^{2+} and Na^{+} ions. The magnetic Fe^{2+} ions are connected exclusively by diamagnetic vanadate units. The three local symmetries of $[FeO_6]$ depicted in Figs. 1(c) and 1(d) are in first approximation D_{3d} with the principal axial elongation along [001].

The TL distorts further in an axial manner [29] by shifting the two triangles (top and bottom) receptively whereby a 4+2 "trans" coordination around Fe results. Contrary, for the HL (centered by the slightly smaller and chemically "harder" Mg^{2+}) an angular distortion (tilting of adjacent triangles off the main axis) gives rise to two distinct iron species without any indication of lowering the space group symmetry upon cooling [Figs. 1(a) and 1(b)]. The rigid nature of Mg^{2+} appears to be sufficient to alter the coordination sphere of the Jahn-Teller active Fe^{2+} by a rotorlike tilting of the vanadate (HL). The two distortions refer to a "cis"-type arrangement which produces a slight elongation (Fe1—four oxygen atoms move out and two in) and a compression (Fe2—two oxygen atoms move out and four in). Thereby, the threefold space-group symmetry on the bipartite HL is preserved.

In Fig. 1(b) we show the reduced pseudotrigonal ($Z = 1$) lattice parameter ratio c/a for the monoclinic distorted TL ($a = \frac{1}{2}(a_m/\sqrt{3} + b_m)$ and $c = \frac{1}{2}c_m$) in comparison with the undistorted HL (space group $P\bar{3}$). Note that at temperatures below 250 K the ratios of c/a have the same slope which indicates that only lattice contractions must be considered upon further cooling. For more insights see the Mössbauer spectroscopic results below.

B. ^{57}Fe Mössbauer spectroscopic measurements of $BaNa_2Fe_{2/3}Mg_{1/3}[VO_4]_2$

Mössbauer spectroscopy is a local probe that provides detailed information about the electronic situation of the iron nucleus. The principal hyperfine interactions which essentially describe Mössbauer spectra are: (i) the electric monopole interaction, giving rise to the isomer shift (CS) which relates to the oxidation state of the investigated atom, and (ii) the quadrupole splitting (QS) of the nuclear energy levels which occurs in an electric field gradient (EFG) resulting from the electronic ground state in an anisotropic crystal lattice. In case of magnetically split spectra the QS corresponds to the quadrupole shift (ϵ), see above. The magnetic hyperfine interaction originates from a magnetic hyperfine field (H_{hf}) that acts on the nuclei of the resonant atoms.

Temperature dependent Mössbauer spectra were collected for $BaNa_2Fe_{2/3}Mg_{1/3}[VO_4]_2$ (HL) in the paramagnetic range above 20 K and fitted by Lorentzians (Fig. 2). At ambient temperature and above a single unresolved doublet is observed which indicates a local symmetry of nearly O_h for a single Fe site. This is in line with the x-ray diffraction data shown before. Rapidly, two doublets with rather distinguishable quadrupole splittings [$QS(1, 2)$] develop upon cooling. The doublets originate from the same high-temperature Fe site as their chemical shift (CS) remains identical down to the lowest accessible temperature (3.3 K) of our experiments. The obtained CS values confirm the presence of high-spin Fe^{2+}, for which CS values in a range from 1.2 to 1.4 mm/s are typically found. From additional experiments conducted on oriented paramagnetic samples, the sign of $e^2qQ/2$ is deduced: negative for the Fe1 and positive for the Fe2 site.

At temperatures below 250 K the two doublets are clearly resolved and confirm the presence of two Fe sites in a

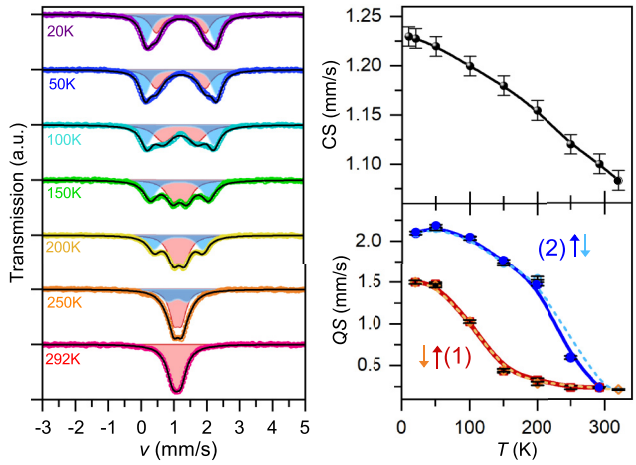

FIG. 2. Left: Mössbauer spectra of $BaNa_2Fe_{2/3}Mg_{1/3}[VO_4]_2$ (HL) with Lorentzian fits to two doublets: Fe1 ($QS1$-red) and Fe2 ($QS2$-blue) shaded areas in a ≈1:1 population ratio below 250 K, measured with increasing temperature. Right: Temperature dependence of the chemical shift for HL (top) and quadrupole splitting (bottom) for the two Fe sites ($QS1$ and $QS2$). The arrows indicate the direction of temperature variations: cooling (↓) and heating (↑).

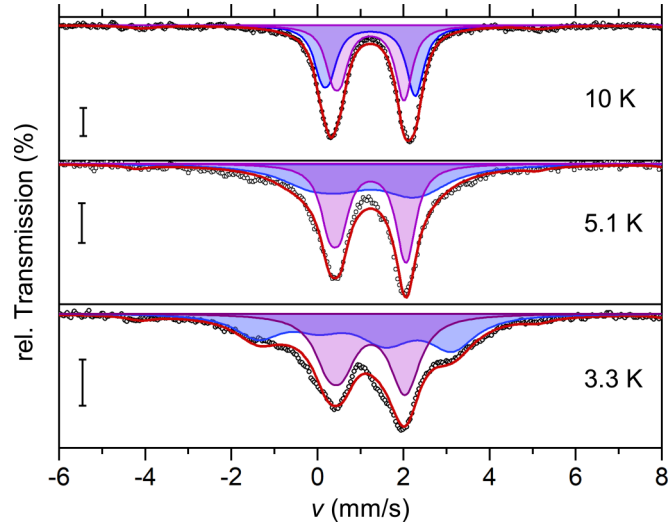

FIG. 3. Mössbauer spectra of $BaNa_2Fe_{2/3}Mg_{1/3}[VO_4]_2$ (HL) fitted by the full static Hamiltonian site analysis for two Fe sites (Fe1-red) and (Fe2-blue), shaded areas in a ≈1:1 population ratio. Red line presents the sum of all spectral components. Bars correspond to a relative transmission scale of 1%.

1:1 ratio. On the time scale of the Mössbauer experiment ($\approx 10^{-8}$ s) an apparent dynamic scenario is resolved. Below 50 K a quasistatic structural situation is present for Fe(1,2). For distinct differences present in $BaNa_2Fe_{1/3}Mg_{2/3}[VO_4]_2$ see Appendix below. Based on the "cis" distortion from D_{3d} symmetry of the $[FeO_6]$ complex along [001], the principal axis of the electric field gradient (EFG) in $P\bar{3}$, we assign the larger quadrupole splitting ($QS2$) to the more compressed coordination sphere of Fe2. The $QS1$ then indicates a further elongation along [001] with a smaller QS for Fe1. This assignment is also in agreement with the work reported in Ref. [42] where an increasing value of QS is linked to a larger shift of Fe from the inversion center of an octahedron. Figure 2 (right) displays the temperature dependence of the hyperfine parameters for HL in the paramagnetic state.

Magnetic fluctuations set in below 20 K as indicated by a developing asymmetrical broadening of the quadrupole spectra. In Fig. 3 and Table I we present the results of our fits using the full static Hamiltonian site analysis. The main result is the development of static components ($T = 3.3$ K) for the Fe2 site with H_{hf} orthogonal to the EFG ($\theta_{hq} = 90°$) whereas for the Fe1 site a significant smaller static hyperfine field remains aligned with the EFG ($\theta_{hq} = 0°$). From respective fits to a dynamical lineshape model we obtained consistent hyperfine parameters and more importantly an estimate of the slow fluctuation rates of $f \approx 7.0$ MHz and $f \approx 22.0$ MHz for Fe2 and Fe1, respectively. Both Fe sites exhibit magnetic hyperfine fields (H_{hf}), which are significantly reduced from typical values of magnetically ordered Fe^{2+} oxides with dominating Heisenberg exchange, e.g., $H_{hf} \approx 380$ kOe [43]. According to Ref. [22] the ground state in trigonal fields is determined by the separation of a singlet $|0>$ and a doublet $|\pm 1>$ and the single-ion anisotropy, $D \approx 10$ K. If the ground state is nonmagnetic then a small H_{hf} is expected and mainly perturbed by mixing in the doublet state through spin-orbit coupling and the respective cis distortion from D_{3d} symmetry.

The presence of two noncollinear hyperfine fields acting on the Fe nucleus and the inherent anisotropy of Fe^{2+} suggests a dominant Dzyaloshinsky-Moriya interaction (DMI) [32,33] on the bipartite lattice. Such a peculiar magnetic exchange precedes the LRO and presumably reduces the ordered moment significantly. To gain more insights into the relevance of such a ferromagnetic component originating from DMI we present magnetization data for the HL in comparison with

TABLE I. Hyperfine parameters obtained from the full static Hamiltonian site analysis for $BaNa_2Fe_{2/3}Mg_{1/3}[VO_4]_2$ (HL) in zero magnetic field: $e^2qQ/2$ (mm/s), H_{hf} (kOe), w (mm/s), and $CS = 1.23$ mm/s.

	(Fe1) with $\theta_{hq} = 0°$			(Fe2) with $\theta_{hq} = 90°$		
T (K)	$e^2qQ/2$	H_{hf}	w	$e^2qQ/2$	H_{hf}	w
3.3	−1.62(1)	11(1)	0.39(1)	1.91(5)	117(2)	0.64(2)
5.1	−1.61(1)	8(1)	0.25(1)	2.00(4)	35(5)	0.39(1)
7.1	−1.56(1)	6(1)	0.23(1)	2.08(1)	7(2)	0.36(1)
10.0	−1.56(1)	6(1)	0.22(1)	2.08(1)	9(1)	0.21(1)

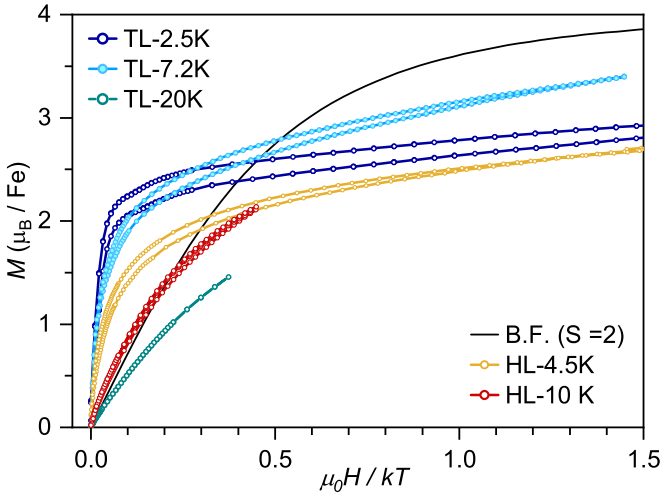

FIG. 4. Magnetization per Fe^{2+} for $BaNa_2Fe[VO_4]_2$ (TL) and $BaNa_2Fe_{2/3}Mg_{1/3}[VO_4]_2$ (HL) at selected temperatures. For comparison the Brillouin function for $S = 2$ is given (black).

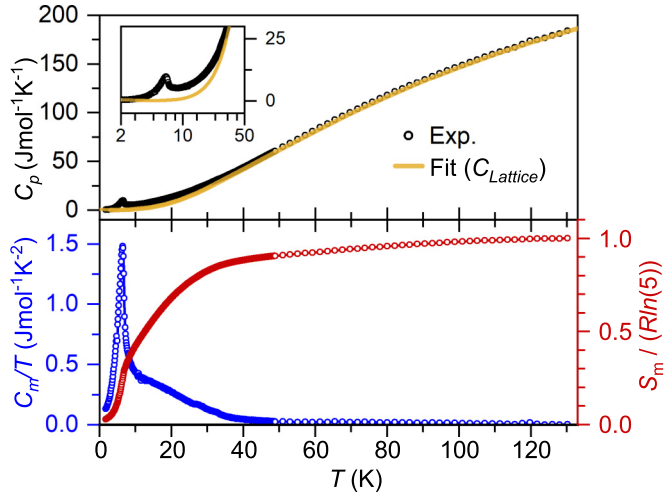

FIG. 5. Top: Total measured specific heat $C_p(T)$ of $BaNa_2Fe[VO_4]_2$ (TL) in zero field. Shown is the fitted lattice contribution $C_{\text{Lattice}}(T)$ (yellow line). The inset shows $C_p(T)$ around the λ anomaly on a logarithmic temperature scale. Bottom: Magnetic part of the specific heat, $C_m(T)$, divided by the temperature (blue) and the spin entropy, $S_m(T)$ per Fe^{2+}, scaled by $Rln(2S + 1)$ (red).

the TL first, before proceeding to our results from Mössbauer spectroscopy for the TL.

C. Magnetization measurements: $BaNa_2Fe[VO_4]_2$ and $BaNa_2Fe_{2/3}Mg_{1/3}[VO_4]_2$

In Fig. 4 we present the field dependent magnetization data for TL and HL at selected temperatures. In the case of the HL a deviation from the idealized magnetization of a $S = 2$ system is observed at 10 K. This corroborates the onset of magnetic fluctuations observed in the Mössbauer spectra reported above and is in line with the conjecture of present anisotropy and the important factor of ferromagnetic exchange. The former relates to the reduced moment at high magnetic fields and the latter to the initial steeper M(H) curve in comparison with the Brillouin function. This feature becomes more pronounced at 4.5 K. The change of M(H) into a rather flat linear field dependence at higher applied fields with an approximate extrapolation of the intercept M(0 kOe) $\approx 1.8\ \mu_B$ provides support that the reduced magnetic moment originates mainly from anisotropy effects inherent to Fe^{2+}.

The magnetization for TL follows, in principle, the same characteristics but with a slightly larger intercept, M(0 kOe) $\approx 2.1\ \mu_B$ at $T = 2.5$ K, consistent with Ref. [30]. Interestingly, at temperatures slightly above the LRO temperature ($T_c = 6.5$ K) the high-field data exhibit a different slope of M(H). This might be taken as an indicator for underlying antiferromagnetic exchange involved. However, the TL ($T = 7.2$ K) and the HL ($T = 4.5$ K) curves show the same linear increase at high applied fields in the fluctuating state. At higher temperatures ($T = 20$ K) the divergence from the Brillouin function is substantial and supports the dominating presence of short ranged antiferromagnetic correlations on the TL. Because only the TL orders above 3 K we will now present the corresponding specific heat measurements in order to gain insights into the released magnetic entropy.

D. Specific heat of $BaNa_2Fe[VO_4]_2$

The total specific heat, $C_p(T)$, of $BaNa_2Fe[VO_4]_2$ (TL) is presented in the top panel of Fig. 5. A λ anomaly occurs at $T_c = 6.5$ K indicative of long-range magnetic order. In order to derive the magnetic contribution to the specific heat, $C_m(T)$, we subtracted the lattice part of the specific heat, $C_{\text{Lattice}}(T)$, which we obtained from a fit to the experimental data. The semiempirical fit model includes the sum of Debye (D) and Einstein (E1, E2) terms (for reference see Ref. [44]): $C_{\text{Lattice}}(T) = C_D(T,\ n = 5,\ \theta_D = 215\ \text{K}) + C_{E1}(T,\ n = 5,\ \theta_{E1} = 370\ \text{K}) + C_{E2}(T,\ n = 4,\ \theta_{E2} = 800\ \text{K})$. The total number of atoms per formula unit amounts to $n_{\text{total}} = 14$ and n represents the corresponding degrees of freedom. θ_{Fe} per Fe site was obtained from a fit to the normalized spectral areas derived from Mössbauer data. To relate this microscopic value of $\theta_{\text{Fe}} = 300$ K to the lattice part of the thermodynamic quantity of the low temperature lattice contribution to the specific heat, we consider an effective environment of coordinatively bound oxygen with a typical covalency factor of $k = 0.8$ for $3d$ ions and the reduced mass ($\sqrt{m_{\text{Fe}}/m_{[\text{FeO}_6]}}$) which then yields $\theta_D = 215$ K.

In Fig. 5 (bottom panel) we show the derived $C_m(T)/T$ data along with the magnetic entropy $S_m(T)$ normalized to the spin entropy for a $S = 2$ system. Below 50 K a significant amount of spin entropy is released and associated with short-range magnetic exchange on the TL. Thus, we expect to find enhanced magnetic fluctuations by the local probe of Mössbauer spectroscopy, see below. The steep increase of C_m below 10 K signalizes the onset of static magnetic order with ≈35% spin entropy involved. This corresponds well to the spontaneous magnetization values at M(0 kOe) given above. Measurements in applied magnetic fields up to 1 T (not shown) shift the λ anomaly to higher temperatures while the feature rapidly smears out, which is indicative of reduced fluctuations and increasing ferromagnetic interactions involved in the static magnetic order.

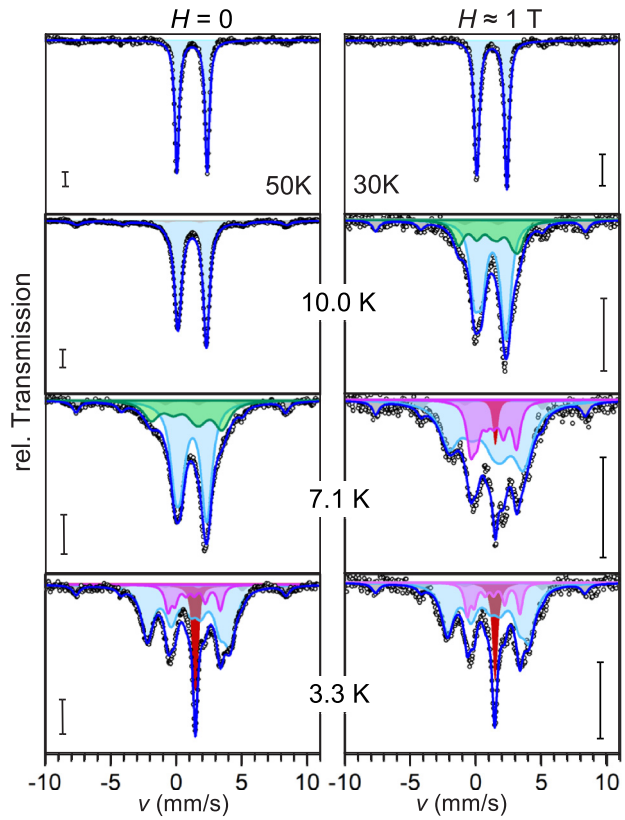

FIG. 6. Mössbauer spectra of $BaNa_2Fe[VO_4]_2$ (TL) at selected temperatures measured in a consecutive heating mode, (left) zero field and (right) in applied magnetic field of $H \approx 1$ T. Black circles represent the experimental data on a relative transmission scale of 1% (bars); the fitted total spectra are depicted by blue lines. Three Fe sites are resolved: main component PS1 (cyan, $\theta_{hq} = 90°$), static PS2 (green, $\theta_{hq} = 90°$ and magenta, $\theta_{hq} = 0°$), quasisuperparamagnetic PS3: red. A gray shaded sextet corresponds to a minor impurity (magnetite).

E. ^{57}Fe Mössbauer spectroscopic measurements of $BaNa_2Fe[VO_4]_2$

Temperature-dependent Mössbauer studies have been reported for Fe^{2+} in the paramagnetic state. These studies were devoted to insights into the structural transition from the space group $P\bar{3}$ to $C2/c$ [29]. It has been shown that the TL exhibits a single Fe site at low temperatures with $CS = 1.23$ mm/s which is equal to the one found for the HL, see above. Thus, the chemical environment and effective oxidation state is the same in both cases, see Fig. 1. The spectrum at 50 K reveals a QS of 2.33 mm/s for TL which is comparable with the Fe2 site of the HL. Below 50 K magnetic fluctuations become evident as the spectra in zero field gain an asymmetric broadened lineshape, see measurement at 10 K($H = 0$ T) and 30 K($H = 1$ T) Fig. 6. This observation is in line with the results shown for $C_m(T)$ and $S_m(T)$ above.

The transition from the paramagnetic to the magnetically ordered state can be clearly monitored in further detail by Mössbauer spectroscopic measurements which detect the on-site magnetic effective exchange field on the Fe nucleus. In particular, information on the static and fluctuating state are provided by this local method with a time resolution of 10^{-8} s [28]. First, we will describe the results obtained in zero field before we proceed to the experimental data obtained in applied fields.

The developing magnetic order exhibits peculiar features. Between 50 K and 10 K the spectra can be fitted to a single Fe site which develops a fast fluctuating hyperfine field without the spectral resolution of a magnetic sextet. The $e^2qQ/2$ parameters remain similar to the QS values observed for the paramagnetic spectra of $BaNa_2Fe[VO_4]_2$ [29]. Around 7.1 K the spectra broaden further and can only be fitted using two magnetic subspectra (PS1 and PS2) in a ratio of 2:1, see Fig. 6 and Table II. The magnetic fluctuation frequency of PS1 remains large with $f \approx 245$ MHz. The simultaneously emerging quasistatic sextet (PS2) is characterized by a significant larger H_{hf} and a reduced f of about 2.0 MHz. The latter value amounts to $\approx 1/3$ of the one for the HL(Fe2) at 3.3 K (see above). Both PS1 and PS2 reveal an orientation of their hyperfine fields orthogonal to the EFG.

The further transition into the magnetically ordered state upon cooling below 6.5 K is indicated by a larger hyperfine field on the PS1 sites and a reduced quadrupole shift which then takes values of $\approx QS/2$ at 3.3 K. Indicative for this static magnetically ordered state are two resolved sextets, see Fig. 6 and Table II. Below $\approx$6.5 K three Fe sites (PS1-3) are present with prominent specific features: (i) QS is almost halved for PS1 and strongly reduced for PS2 and PS3; (ii) PS1 and PS2 are static, H_{hf} increases to 190 kOe for PS1 and is slightly reduced for PS2; (iii) PS3 reveals no static magnetic structure; (iv) $\theta_{hq} = 90°$ (PS1), for PS2 a flip from $\theta_{hq} = 90°$ to $\theta_{hq} = 0°$ aligns PS2 with PS3. The integral intensity of the respective subspectra remains at 2:1 for PS1:(PS2 + PS3). For PS3 a fluctuation rate of the magnetic moment with $f \gtrsim 10^3$ MHz at 3.3 K can be estimated, indicating the magnetic decoupling from the remaining magnetically ordered lattice. Such a fluctuation rate is faster than the characteristic time of the experiment ($\approx 10^{-8}$ s) and similar to a superparamagnetic relaxation [45]. The line shape of PS3 is not split into a doublet structure ($QS \approx 0$), therefore a spherical relaxation may be considered for the decoupling process.

From the evaluation of the magnetic subspectra below 6.5 K, it becomes evident that an orthogonal coupling should be considered to involve DMI as the effective exchange. Moreover, the ratio suggest a scenario with 2/3 sites (PS1) forming a honeycomb lattice centered with 1/3 sites (PS2, PS3) which are magnetically decoupled. It should be noted that the dynamical site (PS3) has a line width ($w = 0.20(1)$ mm/s) slightly narrower than the Lorentzian lineshape of a doublet in the paramagnetic state. In comparison, the line width of PS1 is increased to $w \approx 0.53(2)$ mm/s below 10 K whereas PS2 allies PS3 with only a moderate broadening ($w \approx 0.27(2)$ mm/s).

In order to investigate this peculiar, magnetic order induced decomposition of a single Fe site on the TL into three individual components, we carried out a series of Mössbauer measurements in an external magnetic field ($H \approx 1$ T perpendicular to the incident γ radiation), see Fig. 6, right panel and Table III. All features described above in zero field are corroborated in applied fields. At temperatures below 50 K slow fluctuations are evident and suggest short-range

TABLE II. Mössbauer parameters obtained from full static Hamiltonian site analysis recorded for $BaNa_2Fe[VO_4]_2$ from 3.3 K to 10 K in zero magnetic field. T is given in K, $e^2qQ/2$ in mm/s, H_{hf} in kOe, and θ_{hq} in degrees. $CS = 1.23$ mm/s (PS1, PS2) and $CS = 1.46$ mm/s, $e^2qQ/2 = 0$ (PS3).

	PS 1				PS 2				PS 3
T	$e^2qQ/2$	H_{hf}	θ_{hq}	%	$e^2qQ/2$	H_{hf}	θ_{hq}	%	%
3.3	1.10(1)	190(1)	90	70	0.31 (3)	124(1)	0	18	12
5.1	1.41(4)	186(1)	90	65	0.18(1)	116(1)	0	25	10
6.1	2.85(3)	136(2)	90	70	0.07(8)	98(1)	0	25	5
6.6	2.22(2)	33(2)	90	69	1.67(6)	180(2)	90	28	3
7.1	2.20(1)	19(1)	90	66	2.44(8)	135(3)	90	34	0
10	2.18(1)	12(1)	90	100					

antiferromagnetic correlations which are obviously frustrated on the TL. This low-dimensional short-range ordered state is easily perturbed by external fields in the case of noncollinear interactions like the Y-state of the XY-Heisenberg model [9]. Upon approaching the pre-transitional temperature region, the presumably poorly quenched spin-orbit coupling interaction, inherent to a $S = 2$ spin system, provides the anisotropic component that drives the LRO by a dominating ferromagnetic noncollinear exchange arising from DMI. This feature is corroborated by the shift in applied magnetic fields of the long-range order temperature towards higher temperatures, see spectra at 7.1 K and 10 K for comparison.

IV. DISCUSSION

In this work we present insights into the peculiar magnetic order of $BaNa_2Fe_{2/3}Mg_{1/3}[VO_4]_2$ (HL) and $BaNa_2Fe[VO_4]_2$ (TL) investigated by ^{57}Fe Mössbauer spectroscopy. The $S = 2$ magnetic ions (Fe^{2+}) feature a hexagonal (HL) and a triangular lattice (TL), respectively, see Fig. 7. In both cases we find noncollinear magnetic sublattices with rather small hyperfine fields oriented along ($\theta_{hq} = 0^\circ$) and perpendicular ($\theta_{hq} = 90^\circ$) to the EFG. The latter is defined by the uniaxial parent space group $P\bar{3}$ representing V_{zz} parallel to [001]. For the HL two Fe sites are observed in line with the bipartite nature of the underlying lattice and the structural angular distortions imposed by the rigid nonmagnetic ion in the center of the hexagon (Mg^{2+}).

The exchange in both cases (HL and TL) involves the cross product of adjacent moments (Fig. 7) which is classified as DMI. The resulting pronounced ferromagnetic exchange is evident and confirmed by magnetic measurements. However, down to 3.3 K rather slow magnetic fluctuations persist on the HL. Based on the obtained H_{hf} parameters one would expect $M(H = 0) \approx 1.3\ \mu_B$ for the spontaneous magnetization, well in line with the field-dependent magnetization data. Contrary, for the TL a λ anomaly observed in specific heat measurements indicates LRO. Here the static magnetization suggests $M(H = 0) \approx 1.8\ \mu_B$ in good agreement with the one based on H_{hf} parameters.

Intriguing are the findings for the TL where 2/3 of the Fe sites are characterized by a static in-plane order on a honeycomb lattice arrangement. The central Fe site (1/3 occupancy) of the TL decouples on the timescale of the Mössbauer experiment and consists of a static (PS2) and a fast fluctuating superparamagneticlike (PS3) component in a 1:1 ratio. The space group in this case is $C2/c$ which presents a distortion variant with almost 90° angles and $a/\sqrt{3} \approx b$. Thereby, the threefold rotation axis is lost in comparison with the HL (see above). Thus, the moments (PS1) adhere to an orthogonal alignment on a slightly distorted honeycomb lattice, see Fig. 7 (bottom, cyan). The magnetic moment arises from a cross product of spins on (PS1) sites which

TABLE III. Mössbauer parameters obtained from full static Hamiltonian site analysis recorded for $BaNa_2Fe[VO_4]_2$ from 3.3 K to 30 K in an applied magnetic field of $H = 1$ T. T is given in K, $e^2qQ/2$ in mm/s, H_{hf} in kOe, and θ_{hq} in degrees. $CS = 1.23$ mm/s (PS1, PS2) and $CS = 1.46$ mm/s, $e^2qQ/2 = 0$ (PS3).

	PS 1				PS 2				PS 3
T	$e^2qQ/2$	H_{hf}	θ_{hq}	%	$e^2qQ/2$	H_{hf}	θ_{hq}	%	%
3.3	1.05(8)	188(2)	90	67	0.32(6)	125(1)	0	18	15
5.1	1.31(8)	184(2)	90	65	0.19(2)	114(1)	0	23	12
7.1	2.74(1)	134(1)	90	67	0.26(2)	108(2)	0	28	5
8.0	2.44(1)	128(2)	90	67	0.11(2)	95(1)	0	32	1
9.0	2.18(1)	21(1)	90	67	2.18(1)	121(1)	90	32	1
10.0	2.16(1)	23(1)	90	68	2.16(1)	102(3)	90	32	0
15.0	2.19(2)	18(1)	90	100					
20.0	2.22(1)	12(1)	90	100					
30.0	2.29(1)	7(1)	90	100					

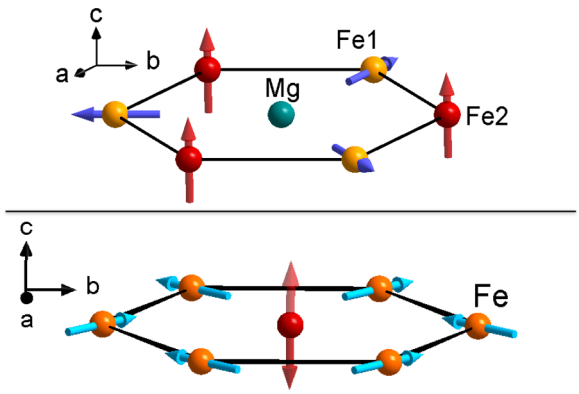

FIG. 7. Representation of magnetic moments at the respective Fe sites in $BaNa_2Fe_{2/3}Mg_{1/3}[VO_4]_2$ (HL, top) and $BaNa_2Fe[VO_4]_2$ (TL, bottom) at 3.3 K.

then align with the central moment (red) either up or down. Presumably this gives rise to the peculiar static/fluctuating nature of the moments on PS2,3 sites in the center of a hexagon.

Now we compare our findings for the TL in the LRO state with the reported neutron diffraction data [30]. Neutron diffraction experiments have not resolved the underlying dynamics and therefore present an averaged picture on longer time scales. The reported magnetic structure [30] contains two alternating stacked layers with derived magnetic moments: $m_a = -1.8(3)\ \mu_B$, $m_b = \pm 3.6(2)\ \mu_B$, and $m_c = 2.5(3)\ \mu_B$. The change in sign for m_b leads to a layer with magnetic moments canted off the c axis and a second one with tilted moments off the ab plane. This averaged translationally periodic magnetic structure neither resolves the site specific information nor the ratio obtained from the local probe experiment presented here. In Fig. 7 (bottom panel) we show the alternating moments using m_a and $\pm m_b$ on a single layer. This scenario represents the PS1 site (cyan) with a noncollinear (orthogonal) in-plane orientation of magnetic moments. The out-of-plane moment then results from DMI. Further coupling to the static and fluctuating PS2, PS3 sites impact the angular (mis)alignment of m_c with the c axis.

The last point we address is concerned with the dynamics on the TL below 50 K. From the specific heat evaluation a large portion of spin entropy is released between 6.5 and 50 K. Since we only observe a single Fe site in this range it seems safe to conclude that all Fe species are participating in the in-plane magnetic exchange. Persisting fluctuations hint to noncollinear but yet not orthogonal orientations of magnetic moments and therefore predominating antiferromagnetic exchange. This scenario on the TL presumes an intrinsic frustration which is lifted by the decomposition into the Fe sites PS1-3 described above at pre-transition temperatures below 10 K. Furthermore, the effect of unquenched orbital momenta is probed on the development of distinct electronic ground states of individual Fe sites. Finally, LRO occurs at 6.5 K. Therefore, the TL would fall into the class of a ferrimagnet. As a side note, $LiFePO_4$ contains chains of strongly distorted $[FeO_6]$ polyhedra connected via diamagnetic $[PO_4]$ tetrahedral linkers. In this case antiferromagnetic LRO is observed ($T_N = 52$ K) [46]. This suggests that the broad fluctuating range and the significant lower LRO temperature of $BaNa_2Fe[VO_4]_2$ results from the frustration and noncollinear exchange involving DMI inherent to the $S = 2$ case on the TL.

V. CONCLUSIONS

We confirm that an axial ("trans") distortion of the $[FeO_6]$ polyhedron on the distorted TL ($BaNa_2Fe[VO_4]_2$) leads to a long-range magnetically ordered ground state. The presence of anisotropy and unquenched orbital momenta for Fe^{2+} however results in the magnetic decomposition of an antiferromagnetic TL. The spin dynamics are intriguing below 10 K and only slowing down to a static case for 2/3 of all Fe sites. LRO stems from additional ferromagnetic exchange as a result of DMI in this case. Although DMI prevails an important factor of the exchange on the HL, the twofold "cis" distortions (Fe1, Fe2) destabilize LRO further via alternating noncollinear magnetic moments which preserve angular degrees of freedom arising from the cross product of adjacent spins. Slow dynamic magnetic fluctuations on different time scales persist in this case. In view of a rational search for QSL, the coexistence of ferromagnetic and antiferromagnetic exchange plus a confinement of alternating "cis" distortions of magnetic octahedra should be considered. The latter requires further size optimization of the supporting central diamagnetic ion in the center of the hexagon or modification of the tetrahedral linker (phosphate, vanadate, etc.). It needs to be stressed that the unsupported HL evades this arrangement in favor of a single distortion that involves shifting the Fe position from the center of the $[FeO_6]$ polyhedron along the threefold rotation axis, see $BaFe_2[PO_4]_2$ [47].

ACKNOWLEDGMENTS

A.M. and V.K. thank the Carl-Zeiss Foundation for support and M. Panthöfer for valuable discussions. Experimental assistance of J. Tapp, G. Siegle, and M. Eremets is gratefully acknowledged. The DFG is acknowledged for funding (INST 247/875-1 FUGG).

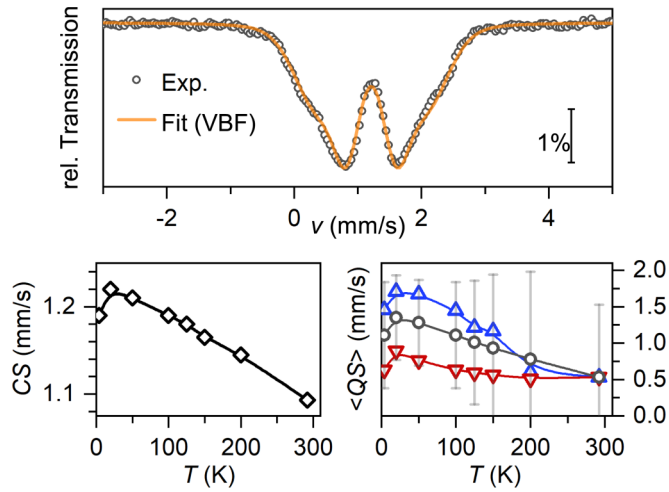

FIG. 8. Mössbauer spectrum of $BaNa_2Fe_{1/3}Mg_{2/3}[VO_4]_2$ at 50 K (top), $CS(T)$ (bottom, left), and (bottom right): $\langle QS \rangle$ with skew $|QS|$ (black, gray), the two components $QS1$ (red) and $QS2$ (blue).

APPENDIX

$BaNa_2Fe_{1/3}Mg_{2/3}[VO_4]_2$ crystallizes as well in the space group $P\bar{3}$. In this case the Mg ions form a honeycomb lattice with Fe^{2+} in the center of the hexagon. Down to 4 K all Mössbauer spectra are paramagnetic and confirm that the Fe sites are isolated from each other (Fig. 8). As expected in this family of compounds, the *CS* is similar to HL ($BaNa_2Fe_{2/3}Mg_{1/3}[VO_4]_2$) and TL ($BaNa_2Fe[VO_4]_2$). However, distinct differences are observed with respect to $BaNa_2Fe_{2/3}Mg_{1/3}[VO_4]_2$ (HL) in terms of the development of the two Fe sites with respective *QS*1 and *QS*2 hyperfine parameters at temperatures below 250 K. While for the HL the two Fe sites are distinct and their subspectra exhibit Lorentzian lineshapes, the hyperfine parameters of the isolated Fe site in $BaNa_2Fe_{1/3}Mg_{2/3}[VO_4]_2$ can only be fitted by a distribution analysis (VBF), here in particular the quadrupole splitting ($\langle QS \rangle$). Overall, the two main components of $\langle QS \rangle$ are smaller than those for HL and TL, suggesting on average reduced distortions from the D_{3d} symmetry. Nevertheless, the Jahn-Teller active Fe^{2+} ion may reduce the degeneracy of the electronic ground state by an off-center shift which results in a component exhibiting a larger *QS*2. This scenario remains dynamic in the entire temperature range, because the rigid [MgO_6] entities constrain the slight tilting of the vanadate only to accommodate the larger Fe^{2+}.

[1] J. E. Greedan, J. Mater. Chem. **11**, 37 (2001).
[2] C. Broholm, R. J. Cava, S. A. Kivelson, D. G. Nocera, M. R. Norman, and T. Senthil, Science **367**, eaay0668 (2020).
[3] J. Knolle and R. Moessner, Annu. Rev. Condens. Matter Phys. **10**, 451 (2019).
[4] L. Messio, S. Bieri, C. Lhuillier, and B. Bernu, Phys. Rev. Lett. **118**, 267201 (2017).
[5] J. Iaconis, C. Liu, G. B. Halsz, and L. Balents, SciPost Phys. **4**, 003 (2018).
[6] R. Islam, C. Senko, W. C. Campbell, S. Korenblit, J. Smith, A. Lee, E. E. Edwards, C.-C. J. Wang, J. K. Freericks, and C. Monroe, Science **340**, 583 (2013).
[7] K. Aoyama and H. Kawamura, Phys. Rev. Lett. **124**, 047202 (2020).
[8] M. F. Collins and O. A. Petrenko, Can. J. Phys. **75**, 605 (1997).
[9] S. Miyashita and H. Kawamura, J. Phys. Soc. Jpn. **54**, 3385 (1985).
[10] L. E. Svistov, A. I. Smirnov, L. A. Prozorova, O. A. Petrenko, L. N. Demianets, and A. Y. Shapiro, Phys. Rev. B **67**, 094434 (2003).
[11] N. E. Amuneke, J. Tapp, C. R. de la Cruz, and A. Möller, Chem. Mater. **26**, 5930 (2014).
[12] J. Tapp, C. R. dela Cruz, M. Bratsch, N. E. Amuneke, L. Postulka, B. Wolf, M. Lang, H. O. Jeschke, R. Valentí, P. Lemmens *et al.*, Phys. Rev. B **96**, 064404 (2017).
[13] S. Lee, R. Klauer, J. Menten, W. Lee, S. Yoon, H. Luetkens, P. Lemmens, A. Möller, and K.-Y. Choi, Phys. Rev. B (unpublished).
[14] M. Mourigal, W. T. Fuhrman, A. L. Chernyshev, and M. E. Zhitomirsky, Phys. Rev. B **88**, 094407 (2013).
[15] L. Chen, D.-W. Qu, H. Li, B.-B. Chen, S.-S. Gong, J. von Delft, A. Weichselbaum, and W. Li, Phys. Rev. B **99**, 140404(R) (2019).
[16] H. A. Jahn and E. Teller, Proc. Roy. Soc. London A **161**, 220 (1937).
[17] R. Nikolova and V. Kostov-Kytin, Bulg. Chem. Commun. **45**, 418 (2013).
[18] A. Möller, N. E. Amuneke, P. Daniel, B. Lorenz, C. R. de la Cruz, M. Gooch, and P. C. W. Chu, Phys. Rev. B **85**, 214422 (2012).
[19] R. Zhong, S. Guo, G. Xu, Z. Xu, and R. J. Cava, PNAS **116**, 14505 (2019).
[20] K. Adachi, K. Takeda, F. Matsubara, M. Mekata, and T. Haseda, J. Phys. Soc. Jpn. **52**, 2202 (1983).
[21] M. Eibschütz, G. R. Davidson, and D. E. Cox, AIP Conf. Proc. **18**, 386 (1974).
[22] M. Eibschütz, M. E. Lines, and R. C. Sherwood, Phys. Rev. B **11**, 4595 (1975).
[23] H. T. Diep, M. Debauche, and H. Giacomini, Phys. Rev. B **43**, 8759 (1991).
[24] C. Stock, L. C. Chapon, O. Adamopoulos, A. Lappas, M. Giot, J. W. Taylor, M. A. Green, C. M. Brown, and P. G. Radaelli, Phys. Rev. Lett. **103**, 077202 (2009).
[25] M. Giot, L. C. Chapon, J. Androulakis, M. A. Green, P. G. Radaelli, and A. Lappas, Phys. Rev. Lett. **99**, 247211 (2007).
[26] A. Zorko, S. El Shawish, D. Arčon, Z. Jagličić, A. Lappas, H. van Tol, and L. C. Brunel, Phys. Rev. B **77**, 024412 (2008).
[27] A. C. Komarek, T. Taetz, M. T. Fernández-Díaz, D. M. Trots, A. Möller, and M. Braden, Phys. Rev. B **79**, 104425 (2009).
[28] F. van der Woude and A. J. Dekker, Phys. Status Solidi B **9**, 775 (1965).
[29] A. Reuß, V. Ksenofontov, J. Tapp, D. Wulferding, P. Lemmens, M. Panthöfer, and A. Möller, Inorg. Chem. **57**, 6300 (2018).
[30] L. D. Sanjeewa, V. O. Garlea, M. A. McGuire, M. Frontzek, C. D. McMillen, K. Fulle, and J. W. Kolis, Inorg. Chem. **56**, 14842 (2017).
[31] M. Bratsch, J. Tapp, A. P. Litvinchuk, and A. Möller, Inorg. Chem. **53**, 4994 (2014).
[32] I. Dzyaloshinsky, J. Phys. Chem. Solids **4**, 241 (1958).
[33] T. Moriya, Phys. Rev. **120**, 91 (1960).
[34] J. R. Morey, A. Scheie, J. P. Sheckelton, C. M. Brown, and T. M. McQueen, Phys. Rev. Materials **3**, 014410 (2019).
[35] A. A. Coelho, TOPAS-Academic V6 (2016).
[36] Ken Lagarec and D. G. Rancourt, Recoil (1998), http://www.physics.uottawa.ca/~recoil.
[37] J. A. Tjon and M. Blume, Phys. Rev. **165**, 456 (1968).
[38] M. Blume and J. A. Tjon, Phys. Rev. **165**, 446 (1968).
[39] S. Horii, A. Ishihara, T. Fukushima, T. Uchikoshi, H. Ogino, T. S. Suzuki, Y. Sakka, J. ichi Shimoyama, and K. Kishio, Sci. Technol. Adv. Mater. **10**, 014604 (2009).
[40] P. Zory, Phys. Rev. **140**, A1401 (1965).

[41] A. Reuß, V. Ksenofontov, J. Tapp, and A. Möller, Z. Anorg. Allg. Chem. **644**, 1849 (2018).
[42] K. K. P. Srivastava, J. Phys. C: Solid State Phys. **19**, 6407 (1986).
[43] C. A. McCammon and D. C. Price, Phys. Chem. Miner. **11**, 250 (1985).
[44] E. Gamsjger and M. Wiessner, Monatshefte fuer Chemie - Chemical Monthly **149**, 357 (2018).
[45] H.-D. Pfannes, J. H. Dias Filho, R. Magalhães Paniago, J. L. López, and R. Paniago, Braz. J. Phys. **31**, 409 (2001).
[46] G. Rousse, J. Rodriguez-Carvajal, S. Patoux, and C. Masquelier, Chem. Mater. **15**, 4082 (2003).
[47] R. David, A. Pautrat, D. Filimonov, H. Kabbour, H. Vezin, M.-H. Whangbo, and O. Mentré, J. Am. Chem. Soc. **135**, 13023 (2013).